Next-to-leading order electroweak corrections to off-shell WWW production at the LHC

Marek Schönherr

Theoretical Physics Department, CERN,
1211 Geneva 23, Switzerland

E-mail: marek.schoenherr@cern.ch

ABSTRACT: Triboson processes allow for a measurement of the triple and quartic couplings of the Standard Model gauge bosons, which can be used to constrain anomalous gauge couplings. In this paper we calculate the next-to-leading order electroweak corrections to fully off-shell $W^-W^+W^+$ production, namely the production of a $\ell_1^- \ell_2^+ \ell_3^+ \bar{\nu}_{\ell_1} \nu_{\ell_2} \nu_{\ell_3}$ final state with $(\ell_i = e, \mu)$, including all triple, double, single and non resonant topologies and interferences of diagrams with all different vector boson (W, Z, γ) intermediate states. We find large cancellations of the electroweak correction to the $q\bar{q}$-induced channel, which includes the exchange of virtual electroweak gauge bosons, and photon-induced jet radiation processes. This accidental compensation is found to be strongly phase space and observable dependent. The resulting corrections in a suitably defined fiducial region thus amount to -2.0%, but rise rapidly for other observables.

Contents

1 Introduction

The precise understanding of the details of the breaking of the electroweak symmetry of the Standard Model is one of the cornerstones of the LHC physics programme. New physics effects, which might play a role in this process, may conveniently be parametrised in terms of effective theories where heavy degrees of freedom are integrated out. Deviations from the Standard Model thus arise as higher-dimensional operators, which can lead to deviations in the triple and quartic couplings of the Standard Model gauge bosons. Deviations from the quartic gauge boson couplings in particular may be well measured in triboson processes, and WWW production offers the largest cross sections. Consequently, both ATLAS and CMS institute searches for trilepton production and ATLAS already used the available data to derive constraints on anomalous gauge couplings [1].

The aim to confront collider data with theorical predictions necessitates precise Standard Model predictions. Especially in the context of new physics searches all sources in the Standard Model known to distort spectra in different regions of phase space need to be accounted for. In this paper we calculate the next-to-leading order electroweak (NLO EW) corrections to off-shell $W^-W^+W^+$ production, namely to trilepton $\ell_1^-\ell_2^+\ell_3^+\bar{\nu}_{\ell_1}\nu_{\ell_2}\nu_{\ell_3}$ with $\ell_i = e, \mu$ signatures, including all triple, double, single and non resonant topologies and interferences of diagrams with all different vector boson (W, Z, γ) intermediate states. The QCD corrections to this process were calculated in [2–4] while the electroweak corrections were known in the literature for on-shell final state W and Z bosons, i.e. WWW and WZZ final states, through [5–8]. The NLO QCD corrections have also been matched to parton showers in [9].

This paper is organised as follows: section 2 briefly summarises the anatomy of trilepton production processes in the context of off-shell triboson production and introduces the tools used in the calculations in this paper. Section 3 then presents the computed cross sections and correction factors to NLO EW accuracy for a variety of important observables before a summary is given in section 4.

$\ell_1^- \ell_2^+ \ell_3^+ \bar{\nu}_{\ell_1} \nu_{\ell_2} \nu_{\ell_3}$						on-shell channels
$e^- e^+ e^+ \bar{\nu}_{\ell_1} \nu_{\ell_2} \nu_{\ell_3}$			$\mu^- \mu^+ \mu^+ \bar{\nu}_{\ell_1} \nu_{\ell_2} \nu_{\ell_3}$			
	$e^- e^+ e^+ \bar{\nu}_e \nu_e \nu_e$			$\mu^- \mu^+ \mu^+ \bar{\nu}_\mu \nu_\mu \nu_\mu$		$WWW + WZZ$
	$e^- e^+ e^+ \bar{\nu}_\mu \nu_\mu \nu_e$	$e^- e^+ e^+ \bar{\nu}_\tau \nu_\tau \nu_e$		$\mu^- \mu^+ \mu^+ \bar{\nu}_e \nu_e \nu_\mu$	$\mu^- \mu^+ \mu^+ \bar{\nu}_\tau \nu_\tau \nu_\mu$	WZZ
$e^- e^+ \mu^+ \bar{\nu}_{\ell_1} \nu_{\ell_2} \nu_{\ell_3}$			$\mu^- \mu^+ e^+ \bar{\nu}_{\ell_1} \nu_{\ell_2} \nu_{\ell_3}$			
	$e^- e^+ \mu^+ \bar{\nu}_e \nu_e \nu_\mu$			$\mu^- \mu^+ e^+ \bar{\nu}_\mu \nu_\mu \nu_e$		$WWW + WZZ$
	$e^- e^+ \mu^+ \bar{\nu}_\mu \nu_\mu \nu_\mu$			$\mu^- \mu^+ e^+ \bar{\nu}_e \nu_e \nu_e$		WZZ
	$e^- e^+ \mu^+ \bar{\nu}_\tau \nu_\tau \nu_\mu$			$\mu^- \mu^+ e^+ \bar{\nu}_\tau \nu_\tau \nu_e$		WZZ
$e^- \mu^+ \mu^+ \bar{\nu}_{\ell_1} \nu_{\ell_2} \nu_{\ell_3}$			$\mu^- e^+ e^+ \bar{\nu}_{\ell_1} \nu_{\ell_2} \nu_{\ell_3}$			
	$e^- \mu^+ \mu^+ \bar{\nu}_e \nu_\mu \nu_\mu$			$\mu^- e^+ e^+ \bar{\nu}_\mu \nu_e \nu_e$		WWW

Table 1.   Break-up of the contributing leptonic channels to trilepton production. Channels with identical topologies and, thus, cross sections are shown in the same row. Thus, only the processes in the first respective row will be referred to in the following tables and figures, while the contribution of the respective identical leptonic channels to the total trilepton production cross section is understood. The last column list the contributing on-shell WWW and WZZ channels in this final state.

2   Trilepton production

2.1   Anatomy of trilepton production processes

In general, trilepton production may be associated with one neutrino (WZ production), three neutrinos (WWW and WZZ production), a $b\bar{b}$-pair and three neutrinos ($t\bar{t}W$ production), a b-quark, a light quark and one neutrino (tZj production), a b-quark, a light quark and three neutrinos ($tWWj$ production), or an even higher number of final state particles. As this publication concerns itself with trilepton production in off-shell triboson processes, this category will be examined in detail in the following.

Trilepton production in the context of off-shell triboson production encompasses all processes of the form $\ell_1^- \ell_2^+ \ell_3^+ \bar{\nu}_{\ell_1} \nu_{\ell_2} \nu_{\ell_3}$ with $\ell_i = e, \mu$. τ lepton final states are not considered here, even though they may lead to similar signatures.[1] As indicated, only $\ell_1^- \ell_2^+ \ell_3^+$ trilepton final states are discussed here. The charge conjugated final state $\ell_1^+ \ell_2^- \ell_3^-$, however, has the same anatomy and computational complexity as the presented case, but the results differ due to the different parton fluxes involved.

$\ell_1^- \ell_2^+ \ell_3^+ \bar{\nu}_{\ell_1} \nu_{\ell_2} \nu_{\ell_3}$ with $\ell_i = e, \mu$ now involves fourteen different lepton channels, of which only six comprise a distinct set of Feynman diagrams. They are listed in table 1. In its last column, this table also states the corresponding triboson channels in the on-shell approximation.

2.2   Calculational setup

In this publication the combination of SHERPA [10, 11] and RECOLA[2] [12, 13] is used to perform all numerical calculations. In this combination SHERPA provides the tree-level matrix elements, infrared subtraction, process management and phase-space integration of

---

[1]The extremely narrow width of the τ facilitates a calculation factorised in production and decay of the same complexity as the calculations presented here (in the limit of a massless τ). As only part of its energy is going into the lepton in its decay, however, τ-channels have generally softer spectra.

[2]The public version 1.2 of RECOLA is used.

	N_{diagrams}		N_{channels}				
	B	R	B		R		
			IS	FS	IS		FS
Process	$q\bar{q}$	$q\bar{q}/q\gamma/\bar{q}\gamma$	$q\bar{q}$	$q\bar{q}$	$q\bar{q}$	$q\gamma/\bar{q}\gamma$	$q\bar{q}/q\gamma/\bar{q}\gamma$
$e^- e^+ e^+ \bar{\nu}_e \nu_e \nu_e$	614	5150	98	992	108	118	4868
$e^- e^+ e^+ \bar{\nu}_\mu \nu_\mu \nu_e$	222	1804	88	388	98	103	1706
$e^- e^+ \mu^+ \bar{\nu}_e \nu_e \nu_\mu$	196	1673	98	302	108	118	1581
$e^- e^+ \mu^+ \bar{\nu}_\mu \nu_\mu \nu_\mu$	222	1804	88	388	98	103	1706
$e^- e^+ \mu^+ \bar{\nu}_\tau \nu_\tau \nu_\mu$	111	902	88	194	98	103	853
$e^- \mu^+ \mu^+ \bar{\nu}_e \nu_\mu \nu_\mu$	170	1542	43	216	58	73	1456

Table 2. Number of Feynman diagrams in the Born process (B) and the real emission correction (R) (numbers quoted for both the $q\bar{q}$ and $q\gamma/\bar{q}\gamma$ individually) and the number of associated initial state (IS) and final state (FS) phase space channels, split by their partonic intial states.

all contributions to all processes considered in this publication through its tree-level matrix element generator Amegic [14]. Its inbuilt infrared subtraction [15–23] is performed in the QED generalisation of the Catani-Seymour scheme [24–27] and includes the appropriate initial state mass factorisation counter terms. RECOLA, on the other hand, provides the virtual corrections to all processes, using the COLLIER library [28] for the evaluation of its scalar and tensor integrals. Both programs, SHERPA and RECOLA, are interfaced through the dedicated interface introduced in [19].

All processes in the present paper are calculated including all triple, double, single and non-resonant topologies, as well as all interferences between channels with different vector boson intermediate states (W, Z, γ) where applicable. Most noteworthy here are interferences between WWW and WZZ topologies in channels with same-flavour opposite-sign lepton pairs. To illustrate the computational complexity, the number of contributing Feynman diagrams N_{diagrams} and associated channels in the phase space parametrisation N_{channels} for both the Born and real emission contributions to the NLO EW calculation are listed in table 2. The one-loop computation comprises up to eight-point loop intergrals.

In the case of on-shell $W^- W^+ W^+$ production, the results of [7] were reproduced and an agreement of the relative electroweak corrections to better than one permille has been observed.

3 Results

In this section the numerical results for the production of a $\ell_1^- \ell_2^+ \ell_3^+ \bar{\nu}_{\ell_1} \nu_{\ell_2} \nu_{\ell_3}$ final state $(\ell_i = e, \mu)$ at next-to-leading order accuracy in the electroweak coupling and including all off-shell and interference effects at the LHC at a centre-of-mass energy of 13 TeV are presented. All calculations are performed in the Standard Model using the complex mass scheme [30, 31]. The electroweak parameters are defined in the G_μ-scheme with the fol-

Selection	Cut	Value
general	$p_{\mathrm{T}}(\ell)$	$[20\,\mathrm{GeV}, \infty)$
	$y(\ell)$	$[-2.5, 2.5]$
	$\Delta R(\ell, \ell)$	$[0.2, \infty)$
$\not{p}_{\mathrm{T}} > 20\,\mathrm{GeV}$	$\Delta\phi(\not{p}_{\mathrm{T}}, \ell\ell\ell)$	$[\frac{5}{6}\pi, \pi]$
1, 2 SFOS	$\not{p}_{\mathrm{T}}$	$[50\,\mathrm{GeV}, \infty)$
	$m_{\ell\ell}^{\mathrm{SFOS}}$	$[0, 70\,\mathrm{GeV}] \wedge [100\,\mathrm{GeV}, \infty)$

Table 3. Definition of the fiducial region. All selection cuts are applied to dressed leptons, defined with $\Delta R_{\mathrm{dress}} = 0.1$.

lowing input parameters

$$
\begin{aligned}
G_\mu &= 1.16637 \times 10^{-5}\ \mathrm{GeV}^2 \\
m_W &= 80.385\ \mathrm{GeV} & \Gamma_W &= 2.0897\ \mathrm{GeV} \\
m_Z &= 91.1876\ \mathrm{GeV} & \Gamma_Z &= 2.4955\ \mathrm{GeV} \\
m_h &= 125.0\ \mathrm{GeV} & \Gamma_h &= 0.00407\ \mathrm{GeV} \\
m_t &= 173.2\ \mathrm{GeV} & \Gamma_t &= 1.3394\ \mathrm{GeV} \ .
\end{aligned}
$$

In this scheme, the electromagnetic coupling is defined as

$$
\alpha = \left| \frac{\sqrt{2}\, G_\mu\, \mu_W^2\, \sin^2\theta_{\mathrm{w}}}{\pi} \right| , \tag{3.1}
$$

where the complex mass of particle i and the weak mixing angle are defined, respectively, as

$$
\mu_i^2 = m_i^2 - \mathrm{i}\Gamma_i m_i \qquad \text{and} \qquad \sin^2\theta_{\mathrm{w}} = 1 - \frac{\mu_W^2}{\mu_Z^2} \ . \tag{3.2}
$$

The virtual amplitudes are renormalised correspondingly.

The calculation is performed in the five-flavour scheme, i.e. the bottom quark is assumed massless and, subsequently, also considered as a proton constituent. Correspondingly, the NNPDF3.1 NLO PDF set is used [32] including QED effects (at $\mathcal{O}(\alpha)$, $\mathcal{O}(\alpha_s\alpha)$ and $\mathcal{O}(\alpha^2)$) in the parton evolution in the LUXqed scheme [33, 34], interfaced through LHAPDF [35].[3] Thus, owing to the increased precision of the photon distribution in this new PDF set, photon induced channels appearing at NLO EW are determined with small PDF uncertainties.

The presented calculation is performed using the following scale choice

$$
\mu_R = \mu_F = 3\, m_W \ . \tag{3.3}
$$

Although this scale choice is not expected to provide a good description of the QCD dynamics of this multiscale process, the electroweak corrections quoted in this paper are largely independent of it. Similarly, the CKM matrix is assumed to be diagonal.

---

[3]To be precise the `NNPDF31_nlo_as_0118_luxqed` PDF set interfaced through LHAPDF-6.2.1 is used.

In the following analysis a set of acceptance cuts, adapted and idealised from [1] and listed in table 3, defines the inclusive fiducial phase space. All selections are applied to dressed leptons, defined through recombining the bare lepton four-momentum with the momenta of all photons in a cone with radius $\Delta R_{\mathrm{dress}} = 0.1$ around it. The fiducial region requires exactly three such dressed leptons that have a transverse momentum larger than $20\,\mathrm{GeV}$ and lie within a rapidity interval of -2.5 to 2.5. Further, any pair of leptons is to be separated by at least $\Delta R(\ell, \ell) = 0.2$. Additional jet activity is suppressed by requiring near back-to-back kinematics of the leptonic system and the missing transverse momentum carried by the neutrinos. If the missing transverse momentum is larger than $20\,\mathrm{GeV}$, where it can be measured reasonably accurate in the LHC experiments, the azimuthal separation of the three-lepton-system and the missing transverse momentum must not be smaller than $\frac{5}{6}\pi$. This is done to both minimise backgrounds from $t\bar{t}W$, tZj and $tWWj$ production as well as to control large higher-order QCD corrections that originate in additional jet emissions and the opening of the respective new channels. At the same-time, they serve to reduce the impact of the photon-induced real emission corrections which were found to be large [7].

As the three different production channels, exhibiting no, one or two lepton pairs of the same flavour and opposite sign of its charge (0, 1 or 2 SFOS), are differently affected by their main background, $WZ \to 3\ell + \nu$ production, the set of applied cuts somewhat differs between them. In the case that no SFOS lepton pair is present, no WZ background is present either and no further cut is applied. In the 1 and 2 SFOS case, however, a region around each Z boson resonance is excluded by demanding the invariant mass of every SFOS lepton pair to lie outside the interval $(70\,\mathrm{GeV}, 100\,\mathrm{GeV})$. A supplementary cut on the missing transverse momentum, requiring it to be larger than $50\,\mathrm{GeV}$, further suppresses the WZ backgrounds. The complete analysis has been implemented in RIVET [36].

In the following, we first present inclusive cross sections before moving on to differential distributions in section 3.2. In both cases, we detail the respective electroweak corrections, δ_{EW}, and its disassembly into the respective partonic channels, $\delta_{q\bar{q}}^{\mathrm{EW}}$ and $\delta_{q\gamma/\bar{q}\gamma}^{\mathrm{EW}}$, defined through

$$\langle O \rangle^{\mathrm{NLO\ EW}} \; = \; \langle O \rangle^{\mathrm{LO}} \times \delta_{\mathrm{EW}} \; = \; \langle O \rangle^{\mathrm{LO}} \times \left[\, \delta_{q\bar{q}}^{\mathrm{EW}} + \delta_{q\gamma/\bar{q}\gamma}^{\mathrm{EW}} \,\right] \,. \tag{3.4}$$

In this way, we are able to attribute correctly the respective sizes of genuine (electro)weak corrections (typically negative) and the (positive) photon induced QED-type corrections, despite their extensive *accidental* cancellation, already observed in the on-shell case [7].

3.1 Inclusive cross sections

In this section inclusive cross sections and their NLO EW corrections, divided according to quark- and photon-induced channels, are presented. Further, the combined $\ell_1^- \ell_2^+ \ell_3^+ \bar{\nu}_{\ell_1} \nu_{\ell_2} \nu_{\ell_3}$ $(\ell_i = e, \mu)$ cross section is shown as well as its subdivision into individual leptonic channels. Here, only the unique channels are displayed and all identical channels can be directly inferred by the reader using the identification of table 1. For brevity, it is understood that

	inclusive			
	LO [fb]	δ_{EW}	$\delta_{q\bar{q}}^{\mathrm{EW}}$	$\delta_{q\gamma/\bar{q}\gamma}^{\mathrm{EW}}$
$\ell^-\ell^+\ell^+$	0.4209	$-2.0\,\%$	$-5.2\,\%$	$3.2\,\%$
$e^-e^+e^+$	0.0212	$-3.4\,\%$	$-7.1\,\%$	$3.6\,\%$
$e^-e^+e^+\bar{\nu}_e\nu_e\nu_e$	0.0206	$-3.4\,\%$	$-7.0\,\%$	$3.6\,\%$
$e^-e^+e^+\bar{\nu}_{\mu/\tau}\nu_{\mu/\tau}\nu_e$	0.0006	$-5.4\,\%$	$-9.5\,\%$	$4.1\,\%$
$e^-e^+\mu^+$	0.0938	$-1.4\,\%$	$-5.4\,\%$	$4.1\,\%$
$e^-e^+\mu^+\bar{\nu}_e\nu_e\nu_\mu$	0.0924	$-1.4\,\%$	$-5.4\,\%$	$4.1\,\%$
$e^-e^+\mu^+\bar{\nu}_\mu\nu_\mu\nu_\mu$	0.0007	$-2.9\,\%$	$-6.1\,\%$	$3.2\,\%$
$e^-e^+\mu^+\bar{\nu}_\tau\nu_\tau\nu_\mu$	0.0007	$-2.7\,\%$	$-6.2\,\%$	$3.5\,\%$
$e^-\mu^+\mu^+$	0.0955	$-2.2\,\%$	$-4.6\,\%$	$2.4\,\%$
$e^-\mu^+\mu^+\bar{\nu}_e\nu_\mu\nu_\mu$	0.0955	$-2.2\,\%$	$-4.6\,\%$	$2.4\,\%$

Table 4. Inclusive cross section and electroweak corrections in the fiducial region defined by the cuts of table 3. The remaining processes can be obtained by replacing $e^\pm \leftrightarrow \mu^\pm$ throughout, cf. table 1.

in cases where the neutrino species does not appear in the label of the process they are summed over.

Table 4 now displays the inclusive cross section in the complete fiducial region defined above, cf. table 3. The 0 and 1 SFOS lepton pair channels each contribute roughly 45% of the cross section, while the 2 SFOS channel (also at a disadvantage due to its final state symmetry factor of $\frac{1}{2}$), only contributes about 10%. Similarly interesting is a decomposition in terms of associated processes in the on-shell approximation, cf. table 1. While the pure WWW channel only contributes 45%, the channels with contributions from both the WWW and WZZ channels contribute 53%. The pure WZZ channels, due to the exclusion of resonant $Z \to \ell\ell$ processes through the fiducial cuts, only contribute 1%. It is thus reasonable to conclude that the channels which contain WWW and WZZ resonances are dominated by their WWW topologies. Hence, the fiducial cuts project the trilepton final state well onto WWW production structures.

The size of the electroweak correction varies between different leptonic channels, ranging from -1.4% for $e^-e^+\mu^+\bar{\nu}_e\nu_e\nu_\mu$ to -5.4% for $e^-e^+e^+\bar{\nu}_{\mu/\tau}\nu_{\mu/\tau}\nu_e$. Generally, the pure WZZ channels receive larger corrections than those with a WWW component. This phenomenon has also been noted in the interplay of WW and ZZ channels in dilepton production in [20, 37]. As observed before, the complete electroweak correction suffers from *accidental* cancellations between the genuine (electro)weak corrections in the $q\bar{q}$ channel and the QED-type real jet radiation corrections in the $q\gamma/\bar{q}\gamma$ channels. While the former ranges from -4.6% to -9.5%, the latter compensates with $+2.4\%$ to $+4.1\%$. The largest cancellations are observed in the $e^-e^+\mu^+\bar{\nu}_e\nu_e\nu_\mu$ channel, resulting in the smallest overall correction. Of course, the precise size of the photon-induced corrections is strongly dependent on the precise value and variable used to suppress jet activity. A less restrictive criterion can lead to much larger positive contributions, cf. [7].

	$m(3\ell) > 500\,\text{GeV}$			
	LO [fb]	δ_{EW}	$\delta_{q\bar{q}}^{\text{EW}}$	$\delta_{q\gamma/\bar{q}\gamma}^{\text{EW}}$
$\ell^-\ell^+\ell^+$	0.0338	$-7.7\,\%$	$-16.3\,\%$	$8.6\,\%$
$e^-e^+e^+$	0.0031	$-10.1\,\%$	$-18.3\,\%$	$8.2\,\%$
$e^-e^+e^+\,\bar{\nu}_e\nu_e\nu_e$	0.0029	$-9.9\,\%$	$-18.3\,\%$	$8.3\,\%$
$e^-e^+e^+\,\bar{\nu}_{\mu/\tau}\nu_{\mu/\tau}\nu_e$	0.0001	$-13.4\,\%$	$-19.8\,\%$	$6.4\,\%$
$e^-e^+\mu^+$	0.0081	$-6.8\,\%$	$-16.6\,\%$	$9.8\,\%$
$e^-e^+\mu^+\,\bar{\nu}_e\nu_e\nu_\mu$	0.0079	$-6.5\,\%$	$-16.5\,\%$	$10.0\,\%$
$e^-e^+\mu^+\,\bar{\nu}_\mu\nu_\mu\nu_\mu$	0.0001	$-11.9\,\%$	$-18.0\,\%$	$6.1\,\%$
$e^-e^+\mu^+\,\bar{\nu}_\tau\nu_\tau\nu_\mu$	0.0001	$-11.2\,\%$	$-17.8\,\%$	$6.6\,\%$
$e^-\mu^+\mu^+$	0.0057	$-7.7\,\%$	$-14.8\,\%$	$7.0\,\%$
$e^-\mu^+\mu^+\,\bar{\nu}_e\nu_\mu\nu_\mu$	0.0057	$-7.7\,\%$	$-14.8\,\%$	$7.0\,\%$

Table 5. Cross section and electroweak corrections in the high trilepton invariant mass region defined by adding the requirement $m(3\ell) > 500\,\text{GeV}$ to the fiducial cuts of table 3. The remaining processes can be obtained by replacing $e^\pm \leftrightarrow \mu^\pm$ throughout, cf. table 1.

Table 5 now additionally requires a minimal trilepton invariant mass of $500\,\text{GeV}$. The total trilepton cross section thus drops to 8% of the inclusive value. The importance of the 2 SFOS lepton pair channel almost doubles to 18% while the 1 SFOS lepton pair channel grows only marginally to 48%. The 0 SFOS channel consequently drops to 34%. Again, taken apart by corresponding on-shell channels, the pure WZZ channels increase slightly to 2%, leaving 98% to WWW dominated channels.

The electroweak corrections, through the interplay of $q\bar{q}$ and $q\gamma/\bar{q}\gamma$ channels, show an interesting behaviour in the different channels. While $\delta_{q\bar{q}}^{\text{EW}}$ takes values from -14.8% to -19.8% (generally slightly larger for processes containing WZZ topologies), $\delta_{q\gamma/\bar{q}\gamma}^{\text{EW}}$ ranges from $+6.1\%$ to $+10.0\%$ (generally slightly smaller for processes without WWW topologies), resulting in combined corrections that are substantially smaller. Again, the precise details of this accidental cancellation depend on the precise form of any jet veto applied.

Finally, table 6 shows the inclusive cross sections after requiring a missing transverse momentum of more than $200\,\text{GeV}$ in addition to the fiducial cuts of table 3. Now, the total cross section is reduced to 2.3% of the inclusive value and also its compostion into lepton flavour channels changed markedly. While the 0 SFOS lepton pair channel is reduced to 26%, the 2 SFOS lepton pair channel is raised to 18%. The 1 SFOS channel, with 56%, also contributes more than in the other selections. The contributions of the pure WZZ channels rises to about 6%, leaving the total cross section still being dominated by WWW channels.

The electroweak corrections, at least on the level of the individual contributions are also larger than in the other two selections. Again, $\delta_{q\gamma/\bar{q}\gamma}^{\text{EW}}$ is larger in lepton channels with WWW topologies, ranging here from $+17.1\%$ to 22.2%, whereas the pure WZZ channels exhibit only half that correction. On the contrary, $\delta_{q\bar{q}}^{\text{EW}}$ is relatively uniform with -16.5% to -23.9%. The total correction is thus, again, accidentally small with -3.4%.

| | $\not{p}_{\mathrm{T}} > 200\,\mathrm{GeV}$ | | | |
	LO [fb]	δ_{EW}	$\delta_{q\bar{q}}^{\mathrm{EW}}$	$\delta_{q\gamma/\bar{q}\gamma}^{\mathrm{EW}}$
$\ell^-\ell^+\ell^+$	0.0097	$-3.4\,\%$	$-20.7\,\%$	$17.3\,\%$
$e^-e^+e^+$	0.0009	$-3.1\,\%$	$-23.3\,\%$	$20.2\,\%$
$e^-e^+e^+\nu_e\nu_e\bar{\nu}_e$	0.0007	$-1.8\,\%$	$-23.9\,\%$	$22.2\,\%$
$e^-e^+e^+\nu_e\nu_{\mu/\tau}\bar{\nu}_{\mu/\tau}$	0.0001	$-11.0\,\%$	$-20.1\,\%$	$9.1\,\%$
$e^-e^+\mu^+$	0.0027	$-3.5\,\%$	$-19.9\,\%$	$16.4\,\%$
$e^-e^+\mu^+\nu_\mu\nu_e\bar{\nu}_e$	0.0025	$-3.1\,\%$	$-20.2\,\%$	$17.1\,\%$
$e^-e^+\mu^+\nu_\mu\nu_\mu\bar{\nu}_\mu$	0.0001	$-8.1\,\%$	$-16.5\,\%$	$8.4\,\%$
$e^-e^+\mu^+\nu_\mu\nu_\tau\bar{\nu}_\tau$	0.0001	$-8.0\,\%$	$-16.7\,\%$	$8.7\,\%$
$e^-\mu^+\mu^+$	0.0013	$-3.3\,\%$	$-20.6\,\%$	$17.3\,\%$
$e^-\mu^+\mu^+\nu_\mu\nu_\mu\bar{\nu}_e$	0.0013	$-3.3\,\%$	$-20.6\,\%$	$17.3\,\%$

Table 6. Cross section and electroweak corrections in the high missing transverse momentum region defined by adding the requirement $\not{p}_{\mathrm{T}} > 200\,\mathrm{GeV}$ to the fiducial cuts of table 3. The remaining processes can be obtained by replacing $e^\pm \leftrightarrow \mu^\pm$ throughout, cf. table 1.

3.2 Differential distributions

We now turn the focus of our discussion on differential distributions. Each of figures discussed in the following will consist of four panels. In clockwise direction they are:

a) The upper left panel displays the absolute trilepton cross section at leading and next-to-leading order in the electroweak coupling. The upper of its two ratio plots shows the combined electroweak correction δ_{EW} as well as its two components $\delta_{q\bar{q}}^{\mathrm{EW}}$ and $\delta_{q\gamma/\bar{q}\gamma}^{\mathrm{EW}}$. The lower ratio plot details the composition of the sample into the 0, 1 and 2 SFOS lepton pair channels.

b) The upper right panel presents the 0 SFOS lepton pair channel. As this channel has only one subchannel, it is not further subdivided. The ratio displays the composition and size of its electroweak correction.

c) The lower right panel details the 1 SFOS lepton pair channel, and its three distinct subchannels. The three ratio plots show the size and composition of the respective electroweak corrections for each subchannel.

d) The lower left panel shows the 2 SFOS lepton pair channel, and its two distinct subchannels. Both ratio plots demonstrate the size and composition of their respective electroweak corrections.

Figure 1 shows the electroweak corrections for the trilepton invariant mass distribution, both for the complete trilepton final state and broken down for each distinct lepton channel. The first thing to realise is that the large contribution of the 0 SFOS lepton pair channel as well as the subdominance of the 2 SFOS lepton pair channel originate in the application of the rejection of resonant $Z \to \ell\ell$ topologies in the 1 and 2 SFOS lepton pair channels. Especially the 2 SFOS lepton channel is suppressed over wide phase
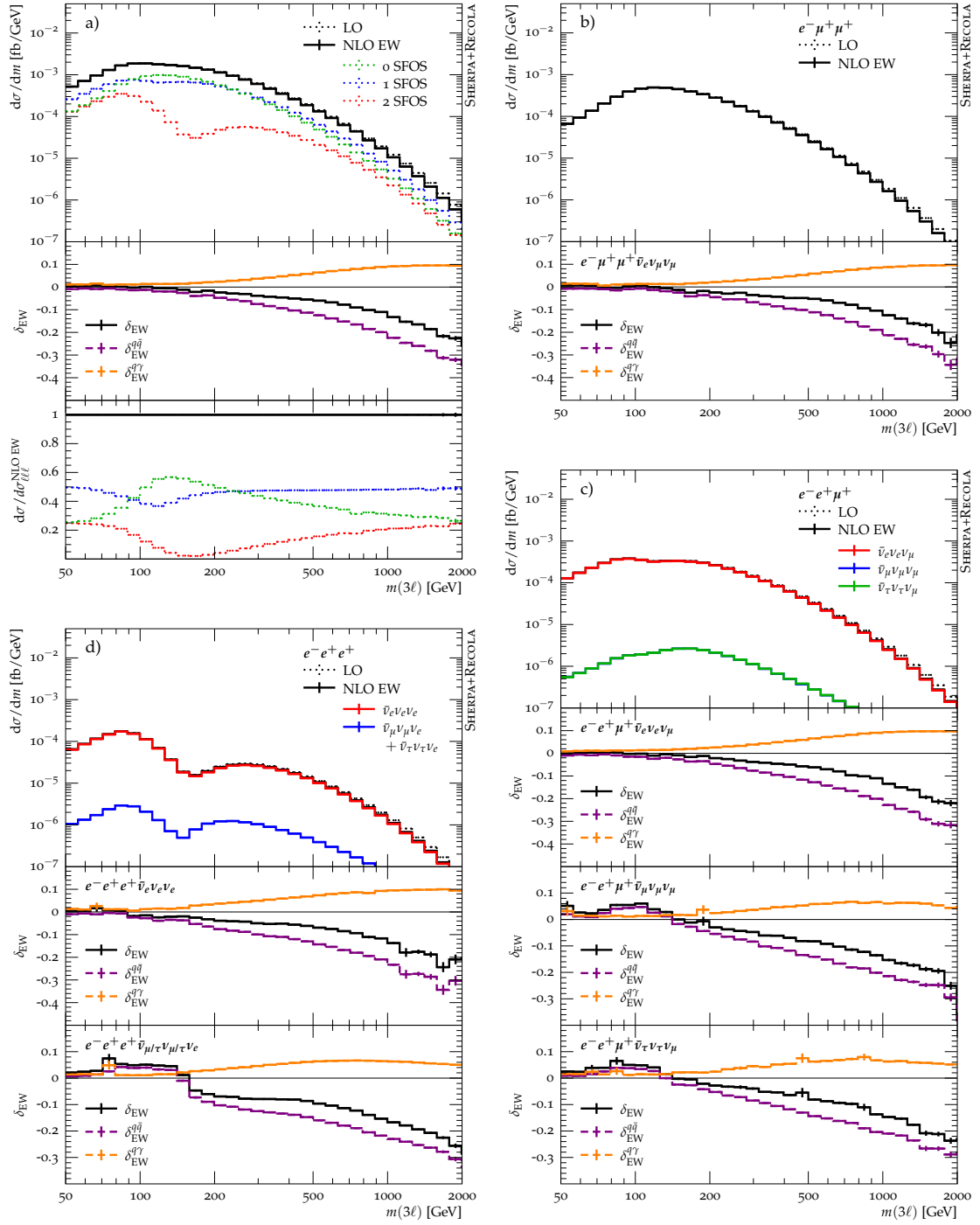
Figure 1. Electroweak corrections to the trilepton invariant mass distribution.

space regions. Secondly, the contribution of the photon-induced real emission correction saturates at high $m_{3\ell}$ (and even decreases beyond the plotted range). Consequently, the combined electroweak corrections $\delta_{\rm EW}$ exhibits its familiar EW Sudakov behaviour in that region. The individual lepton channels all show very similar behaviour, with the onset of the decreasing $\delta_{q\gamma/\bar{q}\gamma}^{\rm EW}$ happening much earlier for the subdominant pure WZZ processes. It is also worth noting that in these channels $\delta_{q\bar{q}}^{\rm EW}$ turns positive at small $m_{3\ell}$, far below the on-shell threshold (at $\frac{1}{2}\left(m_W + 2m_Z\right)$).

The electroweak corrections for the missing transverse momentum distribution is displayed in figure 2. Throughout the spectrum, the contribution of the 1 SFOS lepton pair channel remains approximately constant, while the 2 SFOS lepton pair slowly increases in importance. The 0 SFOS lepton pair channel, however, is the only one contributing at $p\!\!\!/_{\rm T} < 50\,{\rm GeV}$. Thus, although it only contributes $\approx 33\%$ of the cross section above $50\,{\rm GeV}$, maintains a share of 45% of the total fiducial cross section, comparable to that of the 1 SFOS lepton pair channel. The photon-induced corrections increase to maximum of $+25\%$ at $p\!\!\!/_{\rm T} \approx 500\,{\rm GeV}$ and before decreasing rapidly thereafter. Up until that point they, to a very good degree, cancel the genuine electroweak corrections in the $q\bar{q}$ channel, resulting in an almost constant and unnaturally small total $\delta_{\rm EW}$. Only thereafter the electroweak correction rises in the familiar fashion. The $\delta_{q\bar{q}}^{\rm EW}$ on its own, shows this behaviour in the whole range $p\!\!\!/_{\rm T} > 100\,{\rm GeV}$, as expected. In the subdominant lepton channels with only WZZ topologies, where the photon-induced compensation is much smaller, the Sudakov-like shape of the electroweak corrections is much more apparent.

Figure 3–5 finally display the transverse momentum spectra of all three leptons, sorted by $p_{\rm T}$. The general picture is similar for all of them. The photon-induced real emission corrections are smaller than in the missing transverse momentum case and the genuine electroweak corrections in the $q\bar{q}$-channel is larger, resulting in not-substantially disturbed shapes of the total electroweak corrections. At transverse momenta of $500\,{\rm GeV}$ they amount to $\delta_{q\bar{q}}^{\rm EW} \approx -30\%/-40\%/-50\%$ and $\delta_{\rm EW} \approx -20\%/-35\%/-45\%$ for the first/second/third leading lepton.

In the case of the leading lepton they turn positive for very small transverse momenta, below $40\,{\rm GeV}$. In the pure WZZ channels this positive contribution is somewhat larger and extends to slightly higher transverse momenta.

4   Conclusions

In this paper we have calculated the next-to-leading order electroweak corrections to off-shell $W^-W^+W^+$ production, namely to trilepton $\ell_1^-\ell_2^+\ell_3^+\bar{\nu}_{\ell_1}\nu_{\ell_2}\nu_{\ell_3}$ ($\ell_i = e, \mu$) signatures. All triple, double, single and non resonant topologies and interferences of diagrams with all different vector boson (W, Z, γ) intermediate states are included.

We have confirmed that the electroweak corrections exhibit substantial *accidental* cancellations between genuine (electro)weak corrections, dominated by the exchange of virtual electroweak gauge bosons, and the photon-induced real emission corrections that feature an additional jet in the final state, first observed in [7]. The resulting next-to-leading order electroweak corrections amount to approximately -2.0% (-5.2% genuine (electro)weak
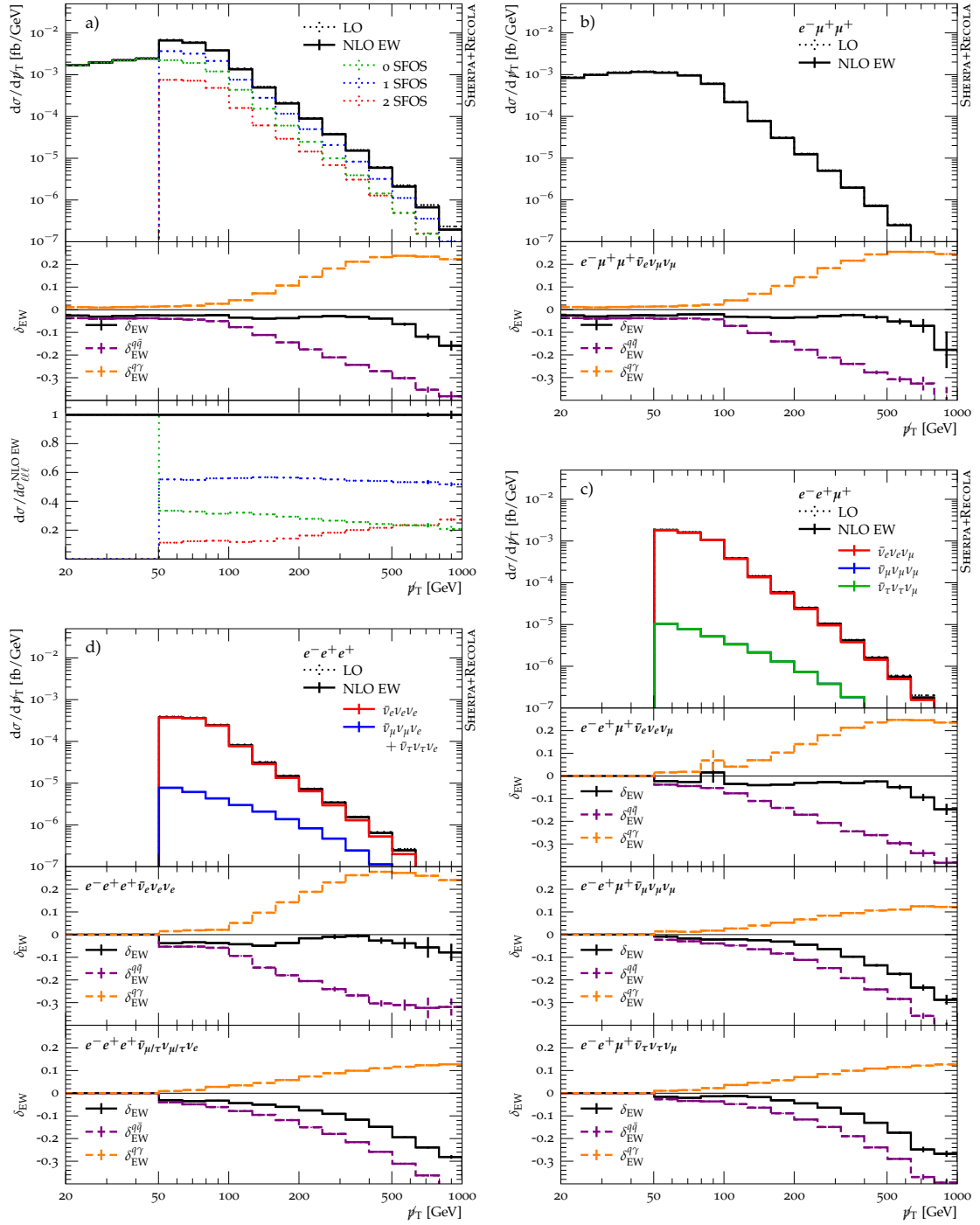
Figure 2. Electroweak corrections to the missing transverse momentum distribution.
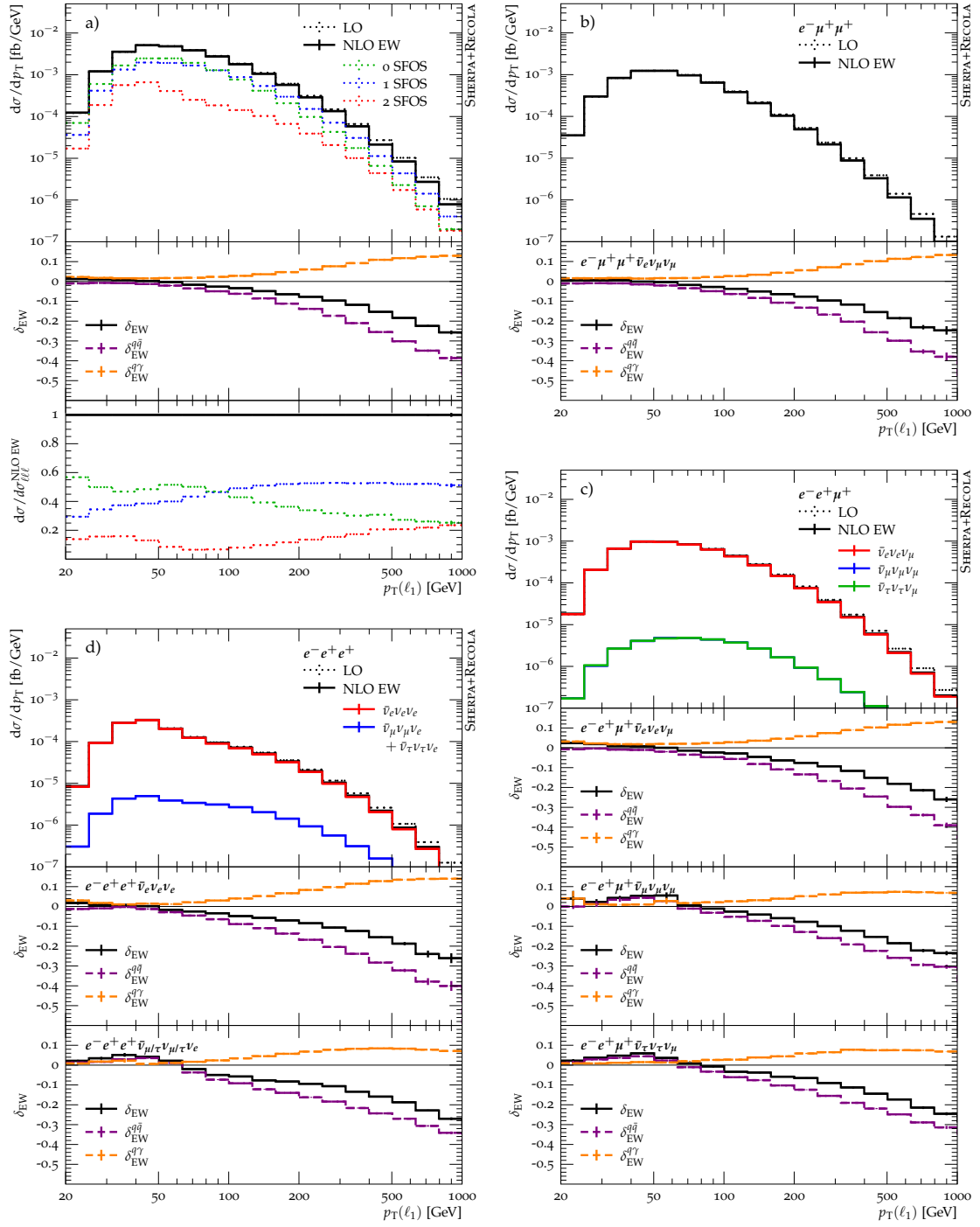
Figure 3. Electroweak corrections to the leading lepton transverse momentum distribution.
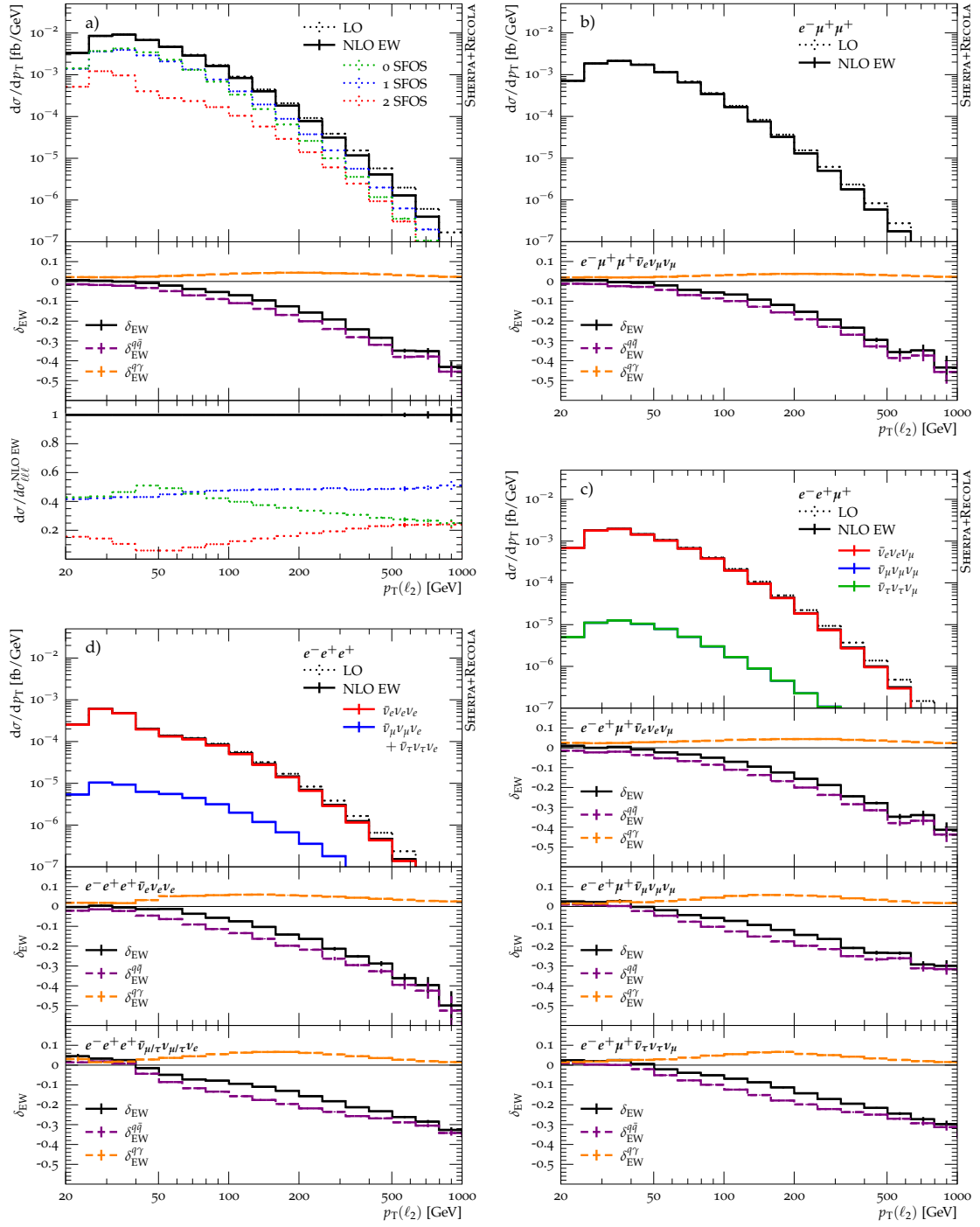
Figure 4. Electroweak corrections to the subleading lepton transverse momentum distribution.
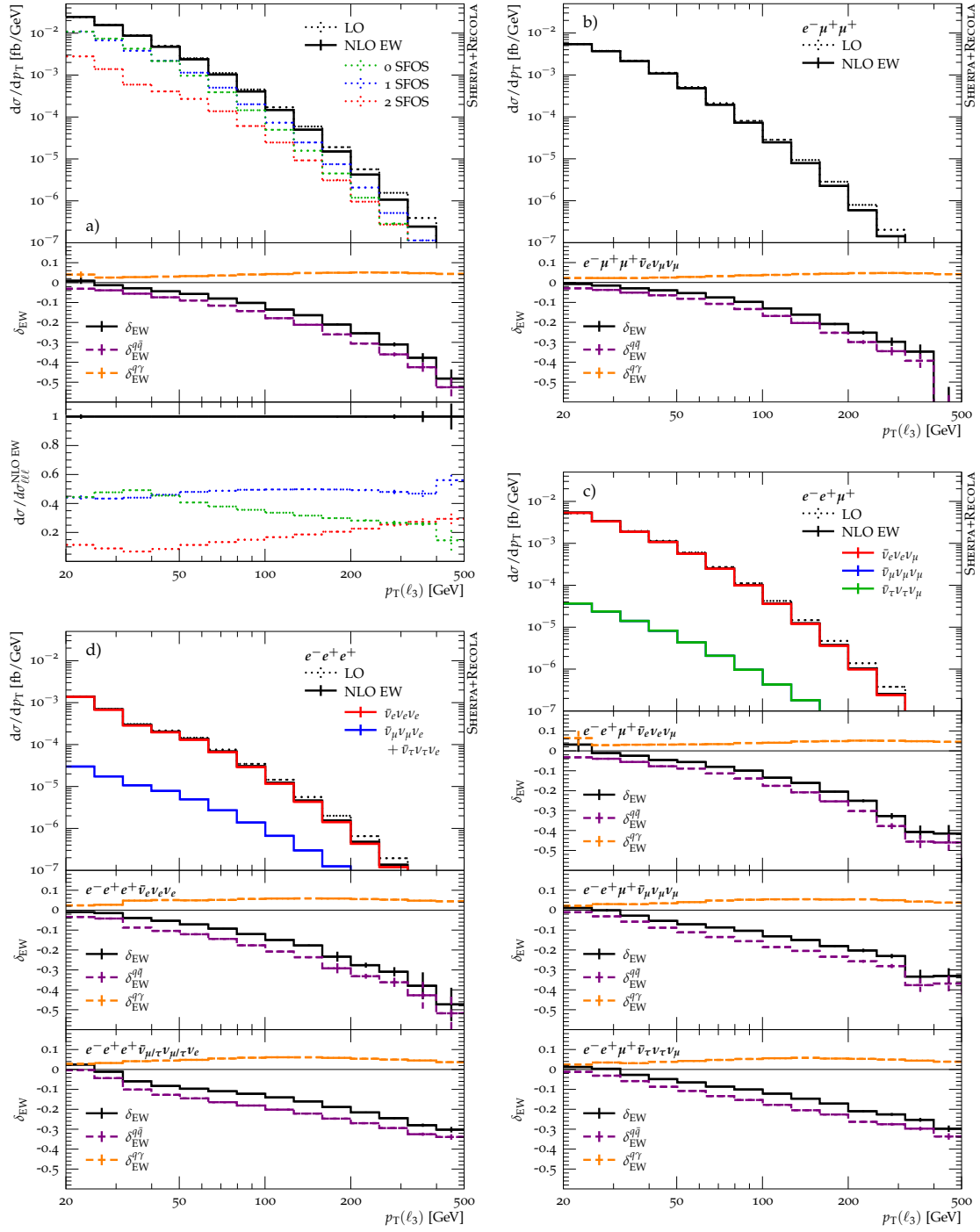
Figure 5. Electroweak corrections to the third-leading lepton transverse momentum distribution.

corrections in the $q\bar{q}$ channel and $+3.2\%$ in the photon-induced jet radiation channel) for the inclusive fiducial cross section with the definition of the fiducial region defined in table 3, which includes a moderate jet veto. It needs to be stressed that the precise impact of the strictly positive contribution from the photon-induced corrections strongly depends on the precise form and value of this jet veto. The electroweak corrections increase rapidly if either the trilepton invariant mass, the missing transverse momentum or any of the lepton transverse momenta are increased. For trilepton invariant masses larger than $500\,\mathrm{GeV}$ they increase to about -7.7% ($-16.3\%+8.6\%$). Similarly, for missing transverse momenta larger than $200\,\mathrm{GeV}$ the complete electroweak corrections amount to -3.4% ($-20.7\% + 17.3\%$). The aforementioned compensation of genuine (electro)weak corrections and photon-induced jet radiation contributions was found to strongly depend on the observable studied. This further emphasises the necessity to compute either contribution exactly.

Further, due to the fully off-shell nature of this calculation, the electroweak corrections in regions like $m_{3\ell} < 3\,m_W$ has now been calculated for the first time. In addition to $\gamma\gamma\gamma$, $\gamma\gamma W$ and $\gamma\gamma Z$ [22] WWW is now the fourth triboson process known to NLO QCD and NLO EW accuracy in the fully off-shell case. Finally, it is worth to stress, that neither of these individually large effects, genuine (electro)weak corrections in the $q\bar{q}$ channel as well as photon-induced jet radiation, is incorporated in any Monte-Carlo event generator in use by the experiments. The presented results detail, that they must be included together consistently as $\mathcal{O}(\alpha)$ corrections to the inclusive process, otherwise important and far-reaching cancellations are missed.

Acknowledgments

References

[1] ATLAS collaboration, *Search for triboson $W^{\pm}W^{\pm}W^{\mp}$ production in pp collisions at $\sqrt{s} = 8\,TeV$ with the ATLAS detector*, *Eur. Phys. J.* **C 77** (2017) 141 [arXiv:1610.05088] [inSPIRE].

[2] A. Lazopoulos, K. Melnikov and F. Petriello, *QCD corrections to tri-boson production*, *Phys. Rev.* **D 76** (2007) 014001 [hep-ph/0703273] [inSPIRE].

[3] T. Binoth, G. Ossola, C.G. Papadopoulos and R. Pittau, *NLO QCD corrections to tri-boson production*, *JHEP* **06** (2008) 082 [arXiv:0804.0350] [inSPIRE].

[4] F. Campanario, V. Hankele, C. Oleari, S. Prestel and D. Zeppenfeld, *QCD corrections to charged triple vector boson production with leptonic decay*, *Phys. Rev.* **D 78** (2008) 094012 [arXiv:0809.0790] [INSPIRE].

[5] Y.-B. Shen et al., *NLO QCD + NLO EW corrections to WZZ productions with leptonic decays at the LHC*, *JHEP* **10** (2015) 186 [*Erratum ibid.* **10** (2016) 156] [arXiv:1507.03693] [INSPIRE].

[6] Y.-B. Shen et al., *NLO QCD and electroweak corrections to WWW production at the LHC*, *Phys. Rev.* **D 95** (2017) 073005 [arXiv:1605.00554] [INSPIRE].

[7] S. Dittmaier, A. Huss and G. Knippen, *Next-to-leading-order QCD and electroweak corrections to WWW production at proton-proton colliders*, *JHEP* **09** (2017) 034 [arXiv:1705.03722] [INSPIRE].

[8] R. Frederix et al., *The automation of next-to-leading order electroweak calculations*, arXiv:1804.10017 [INSPIRE].

[9] S. Hoeche et al., *Triple vector boson production through Higgs-Strahlung with NLO multijet merging*, *Phys. Rev.* **D 89** (2014) 093015 [arXiv:1403.7516] [INSPIRE].

[10] T. Gleisberg et al., *Event generation with SHERPA 1.1*, *JHEP* **02** (2009) 007 [arXiv:0811.4622] [INSPIRE].

[11] E. Bothmann, M. Schönherr and S. Schumann, *Reweighting QCD matrix-element and parton-shower calculations*, *Eur. Phys. J.* **C 76** (2016) 590 [arXiv:1606.08753] [INSPIRE].

[12] S. Actis, A. Denner, L. Hofer, A. Scharf and S. Uccirati, *Recursive generation of one-loop amplitudes in the standard model*, *JHEP* **04** (2013) 037 [arXiv:1211.6316] [INSPIRE].

[13] S. Actis et al., *RECOLA: REcursive Computation of One-Loop Amplitudes*, *Comput. Phys. Commun.* **214** (2017) 140 [arXiv:1605.01090] [INSPIRE].

[14] F. Krauss, R. Kuhn and G. Soff, *AMEGIC++ 1.0: a matrix element generator in C++*, *JHEP* **02** (2002) 044 [hep-ph/0109036] [INSPIRE].

[15] T. Gleisberg and F. Krauss, *Automating dipole subtraction for QCD NLO calculations*, *Eur. Phys. J.* **C 53** (2008) 501 [arXiv:0709.2881] [INSPIRE].

[16] M. Schönherr, *An automated subtraction of NLO EW infrared divergences*, *Eur. Phys. J.* **C 78** (2018) 119 [arXiv:1712.07975] [INSPIRE].

[17] S. Kallweit, J.M. Lindert, P. Maierhöfer, S. Pozzorini and M. Schönherr, *NLO electroweak automation and precise predictions for W+multijet production at the LHC*, *JHEP* **04** (2015) 012 [arXiv:1412.5157] [INSPIRE].

[18] S. Kallweit et al., *NLO QCD+EW predictions for V + jets including off-shell vector-boson decays and multijet merging*, *JHEP* **04** (2016) 021 [arXiv:1511.08692] [INSPIRE].

[19] B. Biedermann et al., *Automation of NLO QCD and EW corrections with Sherpa and Recola*, *Eur. Phys. J.* **C 77** (2017) 492 [arXiv:1704.05783] [INSPIRE].

[20] S. Kallweit, J.M. Lindert, S. Pozzorini and M. Schönherr, *NLO QCD+EW predictions for $2\ell2\nu$ diboson signatures at the LHC*, *JHEP* **11** (2017) 120 [arXiv:1705.00598] [INSPIRE].

[21] M. Chiesa, N. Greiner, M. Schönherr and F. Tramontano, *Electroweak corrections to diphoton plus jets*, *JHEP* **10** (2017) 181 [arXiv:1706.09022] [INSPIRE].

[22] N. Greiner and M. Schönherr, *NLO QCD+EW corrections to diphoton production in association with a vector boson*, *JHEP* **01** (2018) 079 [arXiv:1710.11514] [INSPIRE].

[23] C. Gütschow, J.M. Lindert and M. Schönherr, *Multi-jet merged top-pair production including electroweak corrections*, *Eur. Phys. J.* **C 78** (2018) 317 [arXiv:1803.00950] [INSPIRE].

[24] S. Catani and M.H. Seymour, *A general algorithm for calculating jet cross-sections in NLO QCD*, *Nucl. Phys.* **B 485** (1997) 291 [*Erratum ibid.* **B 510** (1998) 503] [hep-ph/9605323] [INSPIRE].

[25] S. Dittmaier, *A general approach to photon radiation off fermions*, *Nucl. Phys.* **B 565** (2000) 69 [hep-ph/9904440] [INSPIRE].

[26] S. Catani, S. Dittmaier, M.H. Seymour and Z. Trócsányi, *The dipole formalism for next-to-leading order QCD calculations with massive partons*, *Nucl. Phys.* **B 627** (2002) 189 [hep-ph/0201036] [INSPIRE].

[27] S. Dittmaier, A. Kabelschacht and T. Kasprzik, *Polarized QED splittings of massive fermions and dipole subtraction for non-collinear-safe observables*, *Nucl. Phys.* **B 800** (2008) 146 [arXiv:0802.1405] [INSPIRE].

[28] A. Denner, S. Dittmaier and L. Hofer, *Collier: a Fortran-based Complex One-Loop Library In Extended Regularizations*, *Comput. Phys. Commun.* **212** (2017) 220 [arXiv:1604.06792] [INSPIRE].

[29] M. Schonherr and F. Krauss, *Soft photon radiation in particle decays in SHERPA*, *JHEP* **12** (2008) 018 [arXiv:0810.5071] [INSPIRE].

[30] A. Denner, S. Dittmaier, M. Roth and L.H. Wieders, *Electroweak corrections to charged-current $e^+e^- \to 4$ fermion processes: Technical details and further results*, *Nucl. Phys.* **B 724** (2005) 247 [*Erratum ibid.* **B 854** (2012) 504] [hep-ph/0505042] [INSPIRE].

[31] A. Denner and J.-N. Lang, *The complex-mass scheme and unitarity in perturbative quantum field theory*, *Eur. Phys. J.* **C 75** (2015) 377 [arXiv:1406.6280] [INSPIRE].

[32] NNPDF collaboration, V. Bertone et al., *Illuminating the photon content of the proton within a global PDF analysis*, arXiv:1712.07053 [INSPIRE].

[33] A. Manohar, P. Nason, G.P. Salam and G. Zanderighi, *How bright is the proton? A precise determination of the photon parton distribution function*, *Phys. Rev. Lett.* **117** (2016) 242002 [arXiv:1607.04266] [INSPIRE].

[34] A.V. Manohar, P. Nason, G.P. Salam and G. Zanderighi, *The photon content of the proton*, *JHEP* **12** (2017) 046 [arXiv:1708.01256] [INSPIRE].

[35] A. Buckley et al., *LHAPDF6: parton density access in the LHC precision era*, *Eur. Phys. J.* **C 75** (2015) 132 [arXiv:1412.7420] [INSPIRE].

[36] A. Buckley et al., *Rivet user manual*, *Comput. Phys. Commun.* **184** (2013) 2803 [arXiv:1003.0694] [INSPIRE].

[37] A. Bierweiler, T. Kasprzik and J.H. Kühn, *Vector-boson pair production at the LHC to $\mathcal{O}(\alpha^3)$ accuracy*, *JHEP* **12** (2013) 071 [arXiv:1305.5402] [INSPIRE].